

pubs.acs.org/JPCC Article

# Optical Effects on Polarization States in van der Waals Ferroelectric $\alpha$ -In<sub>2</sub>Se<sub>3</sub>

Jacob Parker, Matthew Gabel, Alexander B. C. Mantilla, and Yi Gu\*



Cite This: J. Phys. Chem. C 2023, 127, 22157-22163



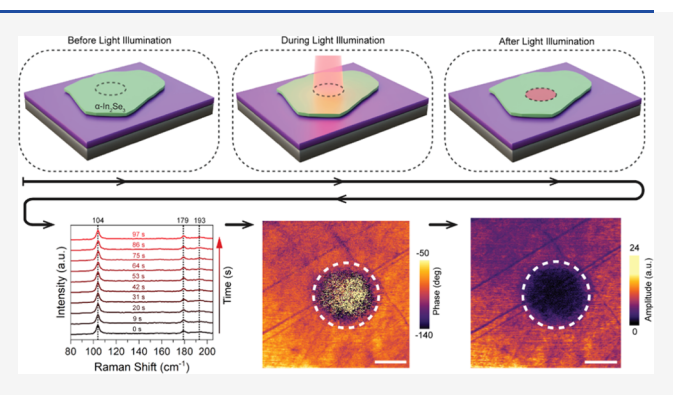
ACCESS I

Metrics & More

Article Recommendations

s Supporting Information

ABSTRACT: Optically controlled ferroelectricity represents a scalable approach to engineering desirable ferroelectric properties for various device applications. With van der Waals ferroelectric  $\alpha$ -In<sub>2</sub>Se<sub>3</sub> being extensively explored for optoelectronic memory and photonic neuromorphic computing technologies, an understanding of the light-ferroelectric interactions is necessary but has not been clearly established. In this study, we show the significant effects of optical illuminations on ferroelectric properties in  $\alpha$ -In<sub>2</sub>Se<sub>3</sub>, particularly the changes from monodomain to disordered polarization states and associated variations of surface electric potentials. We attribute these photoinduced changes to the screening effects from photogenerated carriers that allow for the formation of domain walls and the corresponding multidomain state. These



multidomains are metastable under ambient conditions, persisting for tens of days, but begin to disappear after ~100 days. In addition, they can be returned to the aligned polarization state through external electrical poling. We also demonstrate the reversible optical modulation of device electrical resistance, which is promising for reconfigurable electronics. These findings reveal rich and new phenomena of light-ferroelectric interactions and provide critical microscopic insight that forms the basis for future explorations of novel device concepts based on ferroelectric α-In<sub>2</sub>Se<sub>3</sub>.

#### INTRODUCTION

The ability to control spontaneous electric polarization represents the most important aspect in ferroelectrics and is central to many applications including memory, tunneling diodes, and field-effect transistors. Typically, an external electric field is applied across the material to reverse the polarization. In addition to conventional metal electrodes, using a biased atomic force microscope (AFM) probe as the electric field source is particularly appealing, as it allows for ondemand reconfigurable local domain patterning for desired device functionality.<sup>5-9</sup> However, such an approach is inherently slow and is not readily applicable to large-scale device fabrication. On the other hand, it has been shown 10-14 that light-material interactions in ferroelectrics can drive polarization changes and domain wall motion, opening an alternative and scalable path to modifying domain configurations and associated ferroelectric properties.

The recent emergence of van der Waals ferroelectric materials 4,15-23 provides greater flexibility in integrating materials with distinctive properties into heterostructures with novel functions, such as multiferroicity, polarizationcontrolled electrical conductivity, and ferroelectric field-effect transistors. Among the materials being explored, two-dimensional α-phase In<sub>2</sub>Se<sub>3</sub> (α-In<sub>2</sub>Se<sub>3</sub>) features above-room-temperature ferroelectricity and unique interlinked in-plane (IP) and out-of-plane (OOP) ferroelectric polarizations. <sup>11,24–29</sup> This IP/OOP polarization coupling allows for ferroelectric switching using either an IP or an OOP electric field, and therefore, it is capable of accommodating various device designs and integrations such as planar memristors, ferroelectric field-effect transistors, nonvolatile memory, and neuromorphic computing circuits. 19,30-34 In addition, recent studies have revealed that optical illuminations can tune the electrical conductance of 2D α-In<sub>2</sub>Se<sub>3</sub> nonvolatilely, demonstrating potential for multifunctional devices<sup>35</sup> and photonic synapses.<sup>36</sup> The mechanism of such a phenomenon, however, remains open to debate. Particularly, domain wall motion driven by optical illuminations<sup>36</sup> and polarization reversal due to the neutralization of screening charges by photogenerated carriers<sup>35</sup> have been suggested as the underlying processes.

Here, we show that optical illuminations introduce significant changes to the ferroelectric properties and surface electric potential of  $\alpha$ -In<sub>2</sub>Se<sub>3</sub>; we attribute these photoinduced changes to the emergence of multidomains due to the

Received: July 30, 2023 Revised: October 18, 2023 Accepted: October 18, 2023 Published: November 6, 2023





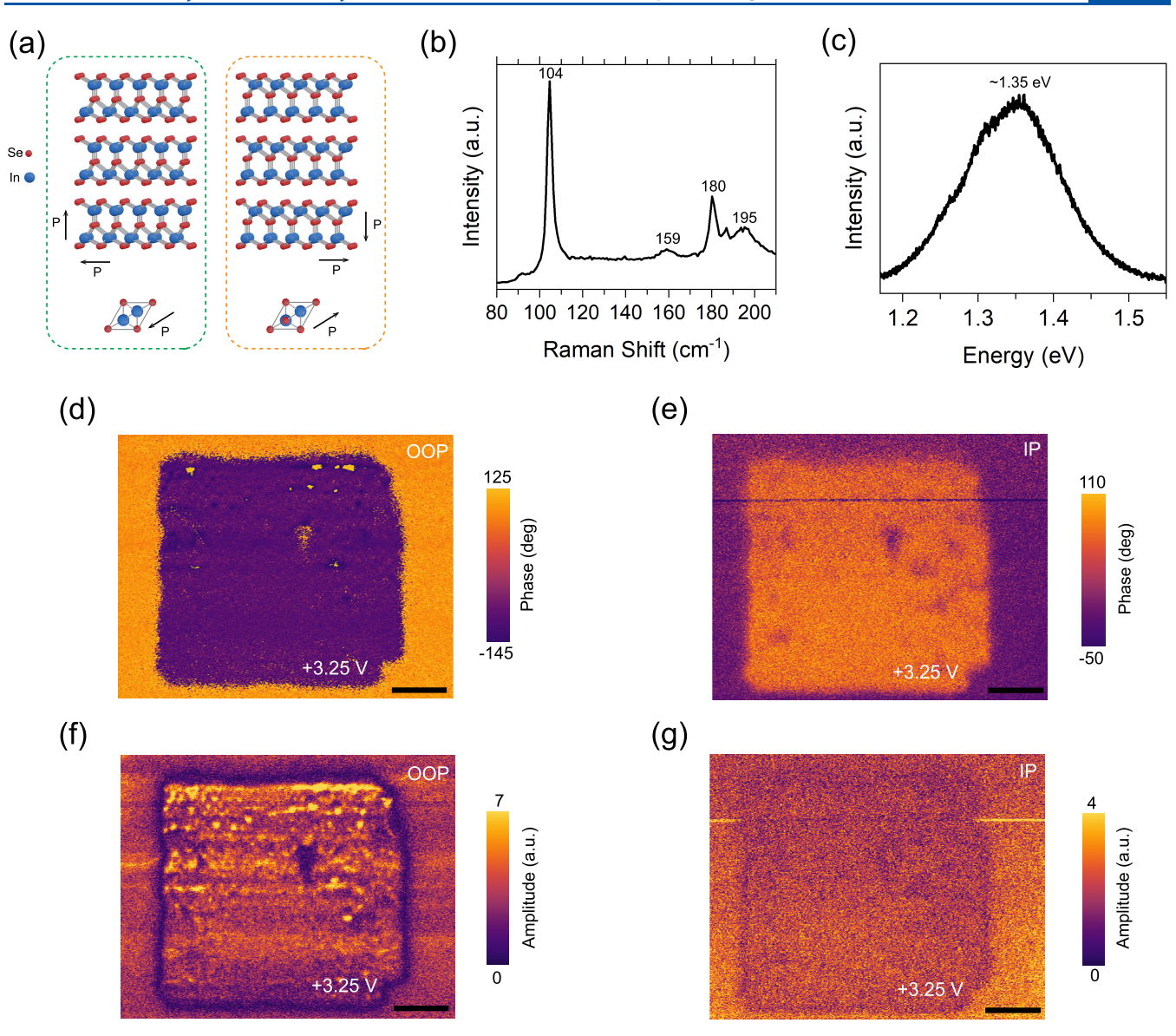


Figure 1. Structural and ferroelectric properties of  $\alpha$ -In<sub>2</sub>Se<sub>3</sub>. (a) Schematic side (top panel) and top (bottom panel) views of  $\alpha$ -In<sub>2</sub>Se<sub>3</sub> crystal structures with two opposite polarization directions (indicated by arrows); (b) Raman and (c) PL spectra of  $\alpha$ -In<sub>2</sub>Se<sub>3</sub> layers; (d-g) OOP-PFM and IP-PFM phase (upper) and amplitude (lower) images of a box pattern written by a biased AFM tip at +3.25 V. Scale bars in panels (d-g) are 200 nm. The  $\alpha$ -In<sub>2</sub>Se<sub>3</sub> layer in panels (d-g) was exfoliated onto a gold-coated substrate. See the Supporting Information for details on substrate parameters.

screening effect from the photogenerated carriers. This multidomain state is metastable under ambient conditions, persisting over approximately tens of days, but begins to revert to the original single-domain state over a longer period of time (~100 days). In addition, external electrical poling can also be used to erase the multidomain state and reverse the polarization to a single-domain state, demonstrating reconfigurability. We also show that the optically illuminated multidomain states can be implemented in device applications by demonstrating reversible optically modulated electrical resistance. These results reveal the new phenomena of light–ferroelectric interactions and associated mechanisms and could enable further novel device concepts such as more advanced reconfigurable memory and neuromorphic computing.

# RESULTS AND DISCUSSION

Figure 1a shows the schematic layered structures of ferroelectric α-In<sub>2</sub>Se<sub>3</sub> that represent two opposite polarization states. The interlinked OOP and IP spontaneous polarizations can be seen from the side and top views of the crystal structure. The Raman spectrum of an as-exfoliated  $\alpha$ -In<sub>2</sub>Se<sub>3</sub> layer (Figure 1b) exhibits main characteristic  $\alpha$ -phase lattice phonon modes<sup>37</sup> at 104, 159, 180, and 195 cm<sup>-1</sup>. Room-temperature photoluminescence (PL) emission at ~1.35 eV is observed (Figure 1c) from these layers, consistent with a recent study<sup>23</sup> that has shown that  $\alpha$ -In<sub>2</sub>Se<sub>3</sub> layers have a band gap at  $\sim$ 1.45 eV. The PL spectra have also been fitted (Figure S1) to reveal any additional peaks in the spectra. To verify the ferroelectricity and intercorrelation between polarization states in  $\alpha$ -In<sub>2</sub>Se<sub>3</sub>, we used a biased AFM tip (experimental details provided in the Supporting Information) to pole the original ferroelectric polarization into the opposite direction and then

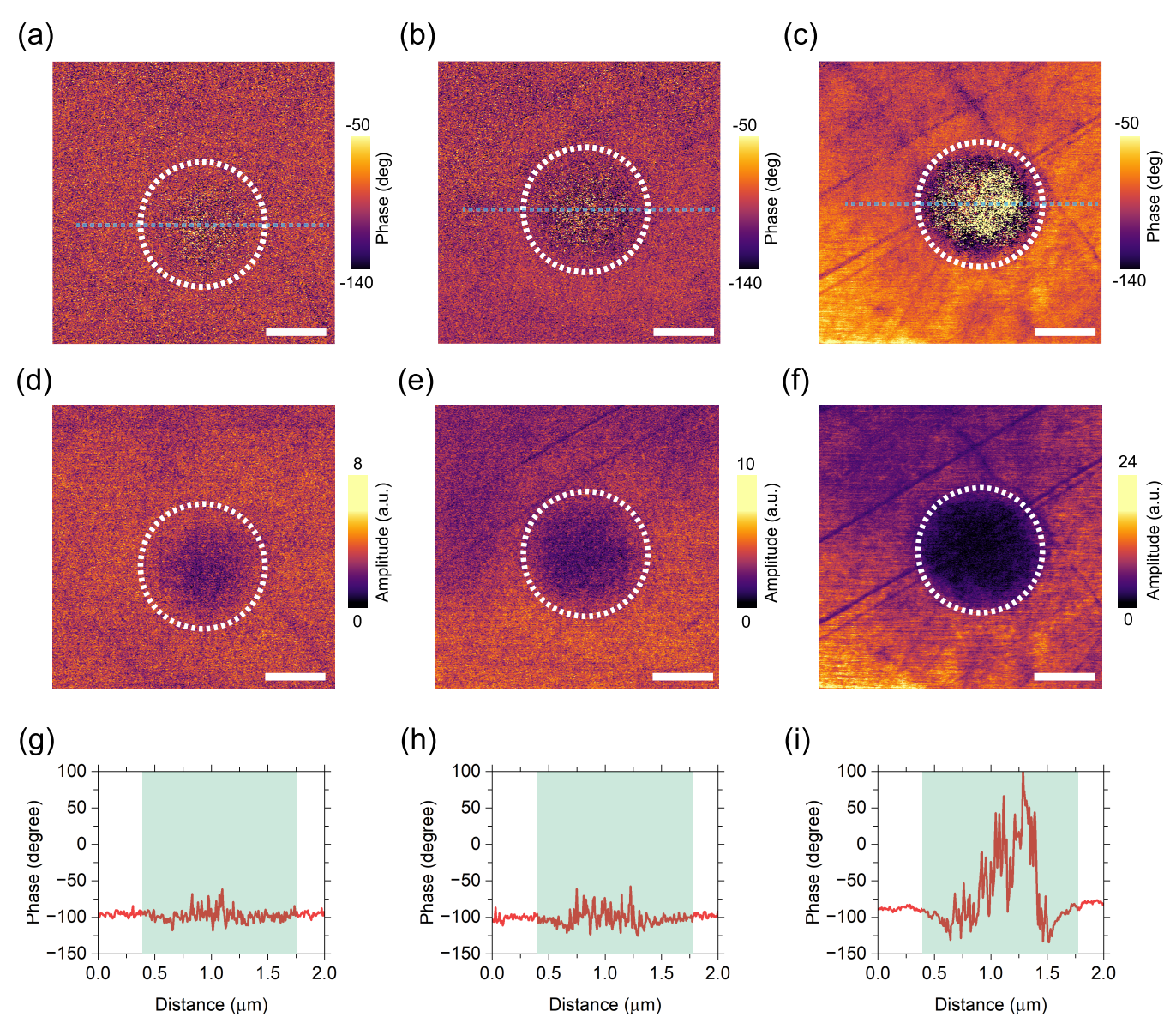


Figure 2. Effects of local optical illuminations. (a–c) PFM phase and (d–f) PFM amplitude images of optically illuminated regions (indicated by circles) with various illumination times (15, 30, and 60 s, respectively) in an  $\alpha$ -In<sub>2</sub>Se<sub>3</sub> layer (67 nm in thickness); (g–i) spatial profiles of the PFM phase across the optically illuminated regions in panels (a–c), respectively, with the shaded areas representing illuminated regions. Scale bars in panels (a–f) are 0.5 μm. The  $\alpha$ -In<sub>2</sub>Se<sub>3</sub> layer was exfoliated on a SiO<sub>2</sub>/Si substrate.

used piezoresponse force microscopy (PFM) to probe the piezoresponse phase and amplitude. As shown in Figure 1d–1g, the square area was poled by scanning the AFM probe biased at +3.25 V. The OOP-PFM (Figure 1d,1f) and IP-PFM (Figure 1e,1g) images show clear correlated phase differences between the original and patterned domain and the diminished piezoresponse amplitude at the domain wall. We further conducted local poling measurements with the OOP-PFM phase and amplitude as functions of the AFM tip bias, showing characteristics consistent with ferroelectric switching (see Figure S2 and discussion).

To investigate the effect of optical illumination, we used 633 nm laser emission focused through a microscope objective as the local optical excitation source. As the laser energy ( $\sim$ 1.96 eV) is above the band gap of  $\alpha$ -In<sub>2</sub>Se<sub>3</sub>, we expect efficient optical absorption and photon–material interactions. Figure 2a–f shows the OOP-PFM phase and amplitude images of an  $\alpha$ -In<sub>2</sub>Se<sub>3</sub> layer exfoliated on a SiO<sub>2</sub> (90 nm)/Si substrate with

multiple locations exposed to local optical illuminations with a laser power density of ~60 kW/cm<sup>2</sup>. We emphasize that no surface topographical changes are observed following the optical illuminations (Figure S3). On the other hand, areas with distinctive piezoresponse amplitude and phase can be clearly observed within the illuminated regions (indicated by circles). Particularly, the PFM amplitude is suppressed within these regions, with the phase signal showing significant fluctuations compared to that from outside the illuminated areas. Similar features are also observed in α-In<sub>2</sub>Se<sub>3</sub> layers exfoliated on Au-coated Si substrates (Figure S4). Figure 2g-i further shows that longer laser exposure times lead to more pronounced variations in PFM phases. The extent of these photoinduced changes is also dependent on the laser power density (Figure S5). Furthermore, we have observed similar photoinduced changes across single domains with opposite polarization directions (Figure S6).

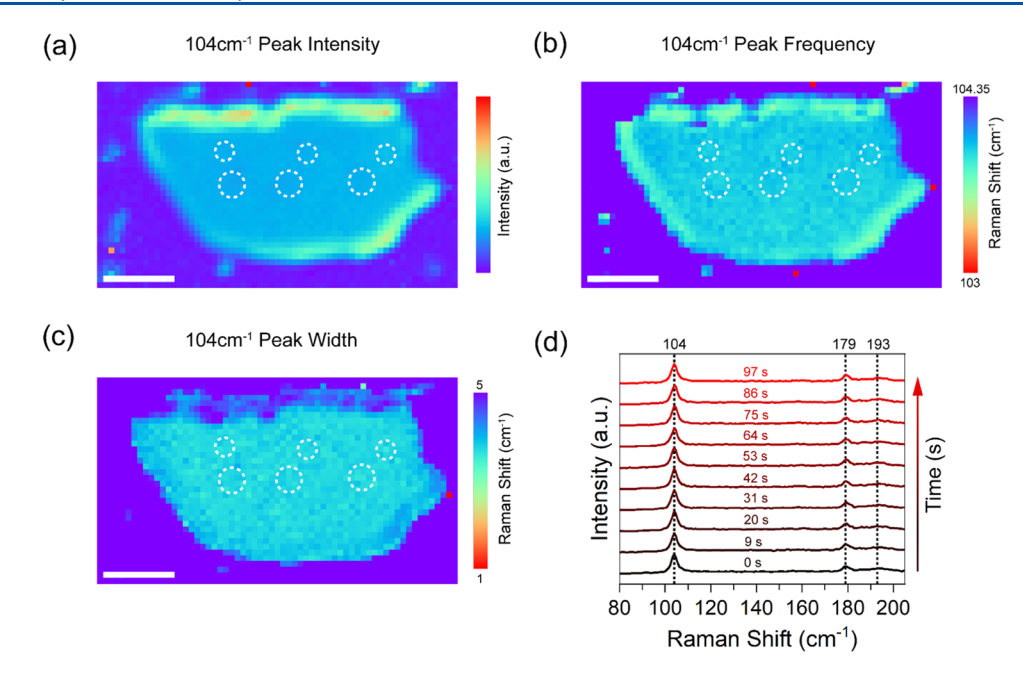


Figure 3. Raman characterization of the illuminated  $\alpha$ -In<sub>2</sub>Se<sub>3</sub> layer and investigation of heating effects. (a–c) Intensity, frequency, and width maps of the characteristic  $\alpha$ -In<sub>2</sub>Se<sub>3</sub> 104 cm<sup>-1</sup> Raman mode with dashed circles indicating the illuminated regions; (d) Raman spectra collected at time intervals during illumination; dashed lines indicate the three main Raman modes (104, 179, and 193 cm<sup>-1</sup>) of  $\alpha$ -In<sub>2</sub>Se<sub>3</sub>. Spectra vertically shifted for clarity. Scale bars in panels (a–c) are 5 μm. The  $\alpha$ -In<sub>2</sub>Se<sub>3</sub> layer was exfoliated on a SiO<sub>2</sub>/Si substrate.

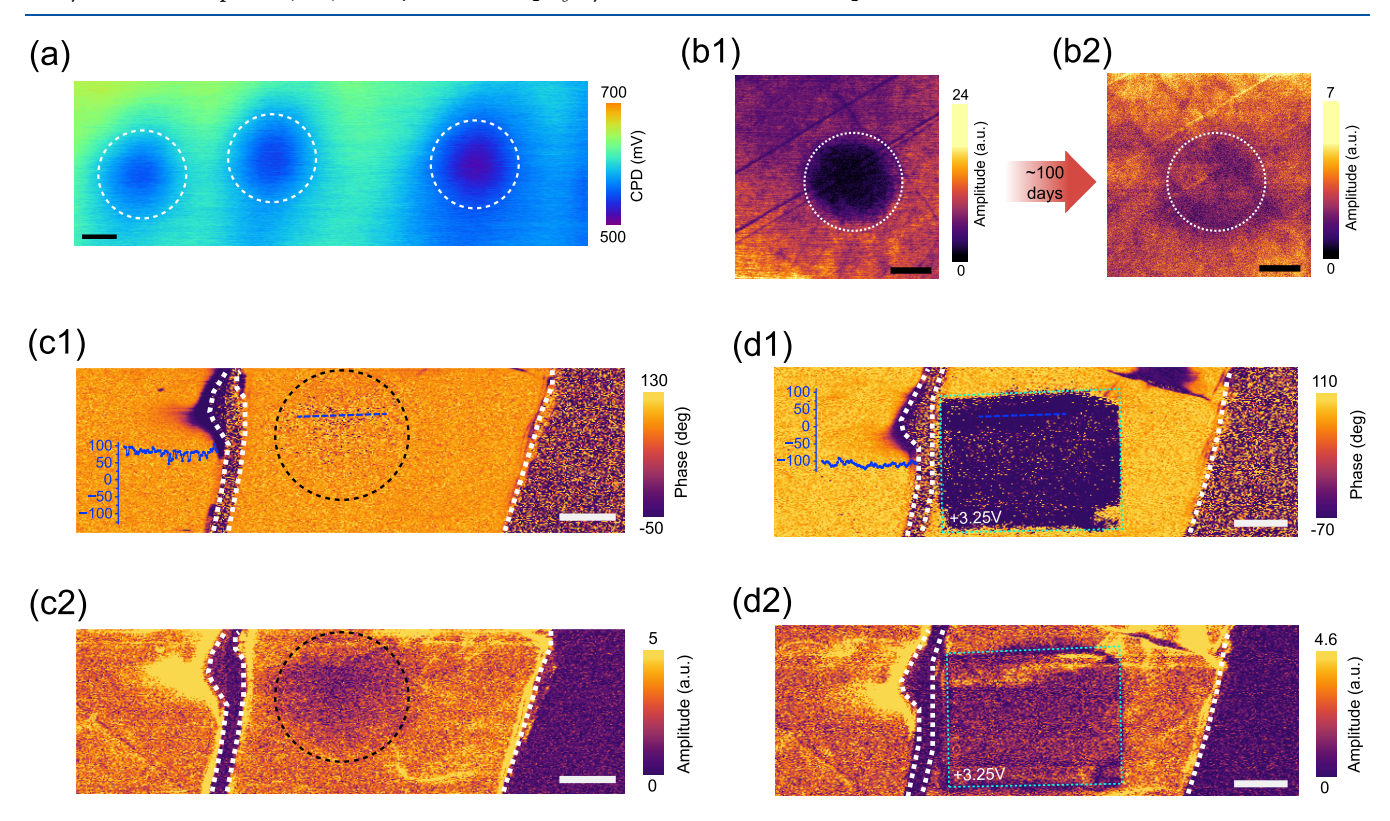


Figure 4. Surface potential measurements, retention, and ferroelectric control of optically illuminated regions. (a) KPFM imaging of illuminated regions in an  $\alpha$ -In<sub>2</sub>Se<sub>3</sub> layer with varying exposure times (from left to right: 60, 90, and 120 s as indicated by dashed circles); (b1) initial OOP-PFM amplitude image after illumination (circled) and (b2) OOP-PFM amplitude image taken after ~100 days, with panel (b1) reproduced from Figure 2f; (c1) OOP-PFM phase and (c2) amplitude of an area illuminated (circled) for 30 s at 30 kW/cm<sup>2</sup>; (d1) OOP-PFM phase and (d2) amplitude of the same area where the illuminated region was poled with an AFM tip biased at +3.25 V to pattern the region into a single-domain state (outlined); insets to panels (c1) and (d1) are the line profiles from the corresponding dashed blue lines. Scale bars are 500 nm. The  $\alpha$ -In<sub>2</sub>Se<sub>3</sub> layers in panels (a, c, d) were exfoliated on gold-coated substrates and the layer in panel (b) was exfoliated on a SiO<sub>2</sub>/Si substrate.

We note that surface topography-related PFM signal variations can be excluded as shown in Figure S3. To probe

the possibility of structural phase changes due to laser heating, <sup>38</sup> we conducted micro-Raman spectroscopy to analyze

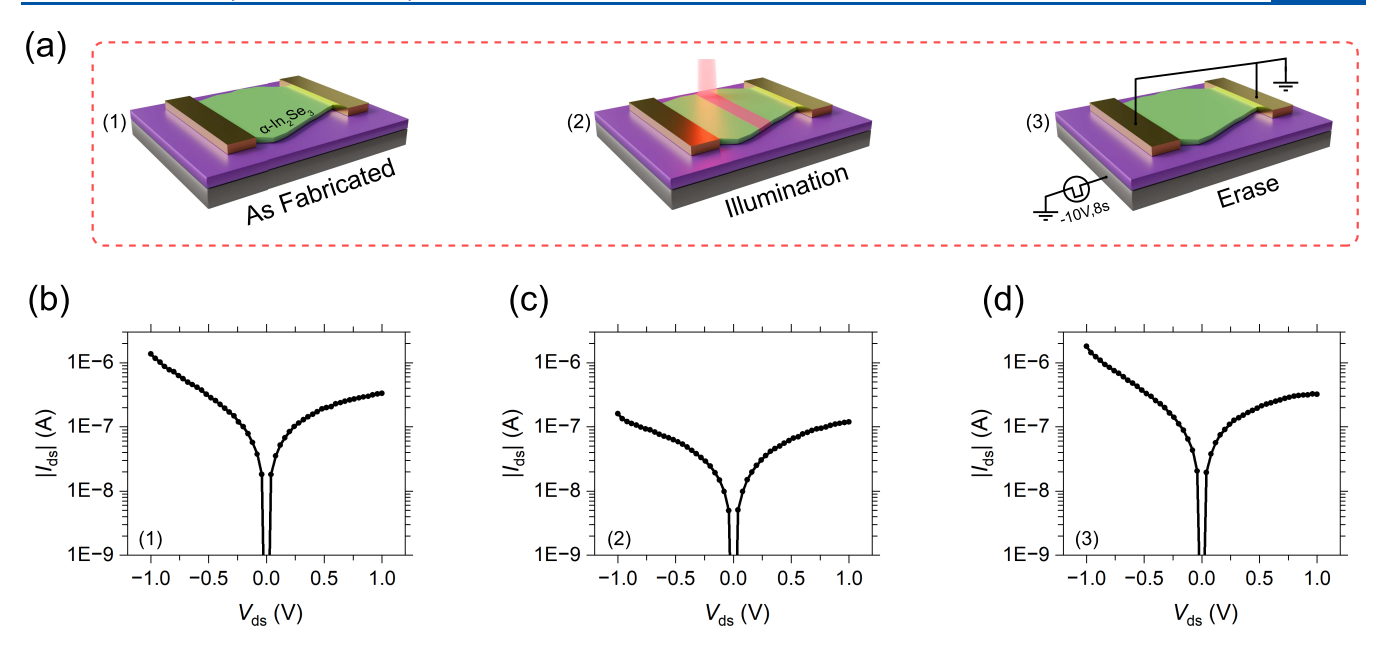


Figure 5. Prototype  $\alpha$ -In<sub>2</sub>Se<sub>3</sub> device. (a) Schematic detailing the device operations; (b) as-fabricated, (c) after-illumination, and (d) after-gate-pulse device current—voltage characteristics. The  $\alpha$ -In<sub>2</sub>Se<sub>3</sub> layer was exfoliated on a SiO<sub>2</sub>/Si substrate.

the intensity, frequency, and full width at half-maximum variations of the main 104 cm<sup>-1</sup> phonon peak of the  $\alpha$ -phase lattice (Figure 3a-c, respectively) across optically illuminated regions (marked by circles) in a layer. The absence of any variations in the main phonon peak characteristics indicates that the lattice structure remains in the  $\alpha$  phase. Additionally, we have also recorded (Figure 3d) the Raman spectra at time intervals during laser illumination with the same power density used in Figure 2. As no significant variations are observed, this indicates minimal laser heating effects. Furthermore, the PFM phase and the amplitude as functions of the tip bias measured inside the optically illuminated regions (Figure S7) still retain the characteristic hysteretic behavior, further confirming the ferroelectric nature of the lattice in the illuminated regions. These observations indicate that the observed changes in the PFM images are due to the photoinduced variations in the local polarization states, which we attribute to the emergence of multidomains. Particularly, as ferroelectric polarization in  $\alpha$ -In<sub>2</sub>Se<sub>3</sub> has the in-plane component, the domain walls are likely to be charged.<sup>36</sup> As such, the formation of new domains, while favored to reduce the energy associated with the depolarization field, 39 needs to overcome the increase in the electric potential energy associated with the charged domain walls.<sup>40</sup> When under optical illumination, this energy barrier to the multidomain state formation is minimized via enhanced screening provided by photogenerated carriers. This allows for the nucleation and growth of new domains, as observed here. This disordered multidomain state is consistent with the observed random fluctuations in the PFM phase spatial profiles (Figure 2g-i) and also accounts for the decrease in the PFM amplitude signals (Figure 2d-f) as the antiparallel polarization states result in a reduced overall polarization magnitude within the area.

Moreover, as ferroelectric polarizations lead to the presence of surface-bound charges at the ferroelectric interface, changes in the polarization direction and magnitude are correlated with variations of the surface-bound charges and thus the surface potential, which can be measured by Kelvin probe force microscopy (KPFM).<sup>41</sup> Our KPFM measurements (Figure 4a;

see also discussion on possible charge trapping effects in Figure S8) demonstrate that the surface potential decreases in the optically illuminated regions, and such changes become more significant with increasing illumination time. This observation is consistent with light-induced multidomain formations with corresponding changes to local polarizations and surface potentials.

We have found that these photoinduced changes under ambient conditions can persist for tens of days ( $\sim$ 40 days) as shown in Figure S9. However, for longer periods of time ( $\sim$ 100 days), we have observed diminishing of photoinduced changes (Figure 4b1,b2). This is consistent with the presence of unscreened charged domain walls that become metastable, and the multidomain state reverts to a single-domain state. The return to a single-domain state can also be achieved by an external poling field. As shown in Figure 4c,d, scanning a biased (at +3.25 V) AFM tip over the layer surface erases the PFM phase contrast associated with the optically illuminated region.

With the capability to define areas with distinctive surface potentials via optically driven multidomain formation, we next explore device applications by demonstrating reversible optical modulation of electrical resistance. Figure 5a,b shows the device schematics and the as-fabricated device current—voltage characteristics, respectively. By scanning a focused laser beam across the channel, we can observe a notable decrease in the device conductance (Figure 5c). This can be attributed to the surface potential variations within the illumination region, which creates potential barriers that impede carrier transport. The device conductance state can be restored to the initial state by applying a -10 V gate voltage pulse for 8 s (Figure 5d), which erases the potential variations through the realignment of the ferroelectric polarizations inside the device channel. 42

# CONCLUSIONS

We have shown that local optical illumination can drastically modify the ferroelectric properties in  $\alpha$ -In<sub>2</sub>Se<sub>3</sub> by randomizing the spatial distribution of polarization state directions. These

optically induced multidomains can persist for a certain period of time (approximately tens of days) and can be reversed to a single polarization state by an external poling field. An important consequence of the changes in the domain configuration is the variations in the surface electric potentials, which evolve with the illuminations. Furthermore, our results show that controlled optical illuminations can be used to define desired electronic patterns in ferroelectric  $\alpha$ -In<sub>2</sub>Se<sub>3</sub> for device applications and open the possibility for further implementations such as in optical memory and memristive and photonic neuromorphic computing. More fundamentally, our results provide critical microscopic insight into light–ferroelectric interactions.

#### ASSOCIATED CONTENT

# **Supporting Information**

The Supporting Information is available free of charge at https://pubs.acs.org/doi/10.1021/acs.jpcc.3c05148. .

 $\alpha$ -In<sub>2</sub>Se<sub>3</sub> fitted PL spectrum; ferroelectric hysteresis of exfoliated  $\alpha$ -In<sub>2</sub>Se<sub>3</sub>;  $\alpha$ -In<sub>2</sub>Se<sub>3</sub> layer topography before and after illuminations; PFM for illuminations on  $\alpha$ -In<sub>2</sub>Se<sub>3</sub>/Au; threshold power density for multidomain state formation; PFM for illuminations on antiparallel domains; ferroelectric hysteresis inside and outside illuminated regions; control experiments on MoS<sub>2</sub>/Au, MoS<sub>2</sub>/SiO<sub>2</sub>, and SiO<sub>2</sub> surfaces; and temporal stability of multidomain states (PDF)

#### AUTHOR INFORMATION

#### **Corresponding Author**

Yi Gu — Department of Physics and Astronomy, Washington State University, Pullman, Washington 99164, United States; ocid.org/0000-0001-7241-9888; Email: yigu@wsu.edu

#### **Authors**

Jacob Parker – Department of Physics and Astronomy, Washington State University, Pullman, Washington 99164, United States; orcid.org/0000-0002-7788-2940

Matthew Gabel – Department of Physics and Astronomy, Washington State University, Pullman, Washington 99164, United States

Alexander B. C. Mantilla – Department of Physics and Astronomy, Washington State University, Pullman, Washington 99164, United States; orcid.org/0000-0002-9262-1351

Complete contact information is available at: https://pubs.acs.org/10.1021/acs.jpcc.3c05148

#### Notes

The authors declare the following competing financial interest(s): Y.G. has equity interest in Klar Scientific.

# ACKNOWLEDGMENTS

Support from the U.S. National Science Foundation (DMR-2004655) is acknowledged.

# REFERENCES

(1) Setter, N.; Damjanovic, D.; Eng, L.; Fox, G.; Gevorgian, S.; Hong, S.; Kingon, A.; Kohlstedt, H.; Park, N. Y.; Stephenson, G. B.; et al. Ferroelectric Thin Films: Review of Materials, Properties, and Applications. *J. Appl. Phys.* **2006**, *100*, No. 051606.

- (2) Martin, L. W.; Rappe, A. M. Thin-Film Ferroelectric Materials and Their Applications. *Nat. Rev. Mater.* **2017**, *2*, No. 16087, DOI: 10.1038/natreymats.2016.87.
- (3) Dawber, M.; Rabe, K. M.; Scott, J. F. Physics of Thin-Film Ferroelectric Oxides. *Rev. Mod. Phys.* **2005**, 77, 1083–1130.
- (4) Si, M. W.; Liao, P. Y.; Qiu, G.; Duan, Y. Q.; Ye, P. D. D. Ferroelectric Field-Effect Transistors Based on Mos2 and Cuinp2s6 Two-Dimensional Van Der Waals Heterostructure. *ACS Nano* **2018**, 12, 6700–6705.
- (5) Xiao, Z. Y.; Song, J. F.; Ferry, D. K.; Ducharme, S.; Hong, X. Ferroelectric-Domain-Patterning-Controlled Schottky Junction State in Monolayer Mos2. *Phys. Rev. Lett.* **2017**, *118*, No. 236801.
- (6) Chen, J.-W.; Lo, S.-T.; Ho, S.-C.; Wong, S.-S.; Vu, T.-H.-Y.; Zhang, X.-Q.; Liu, Y.-D.; Chiou, Y.-Y.; Chen, Y.-X.; Yang, J.-C.; et al. A Gate-Free Monolayer Wse2 Pn Diode. *Nat. Commun.* **2018**, *9*, No. 3143.
- (7) Lipatov, A.; Li, T.; Vorobeva, N. S.; Sinitskii, A.; Gruverman, A. Nanodomain Engineering for Programmable Ferroelectric Devices. *Nano Lett.* **2019**, *19*, 3194–3198.
- (8) Lv, L.; Zhuge, F. W.; Xie, F. J.; Xiong, X. J.; Zhang, Q. F.; Zhang, N.; Huang, Y.; Zhai, T. Y. Reconfigurable Two-Dimensional Optoelectronic Devices Enabled by Local Ferroelectric Polarization. *Nat. Commun.* **2019**, *10*, No. 3331.
- (9) Wu, G.; Tian, B.; Liu, L.; Lv, W.; Wu, S.; Wang, X.; Chen, Y.; Li, J.; Wang, Z.; Wu, S.; et al. Programmable Transition Metal Dichalcogenide Homojunctions Controlled by Nonvolatile Ferroelectric Domains. *Nat. Electron.* **2020**, *3*, 43–50.
- (10) Nova, T. F.; Disa, A. S.; Fechner, M.; Cavalleri, A. Metastable Ferroelectricity in Optically Strained SrTiO3. *Science* **2019**, *364*, 1075–1079.
- (11) Wan, S. Y.; Li, Y.; Li, W.; Mao, X. Y.; Zhu, W. G.; Zeng, H. T. Room-Temperature Ferroelectricity and a Switchable Diode Effect in Two-Dimensional Alpha-In2se3 Thin Layers. *Nanoscale* **2018**, *10*, 14885–14892.
- (12) Vats, G.; Bai, Y.; Zhang, D. W.; Juuti, J.; Seidel, J. Optical Control of Ferroelectric Domains: Nanoscale Insight into Macroscopic Observations. *Adv. Opt. Mater.* **2019**, *7*, No. 1800858.
- (13) Rubio-Marcos, F.; Del Campo, A.; Marchet, P.; Fernandez, J. F. Ferroelectric Domain Wall Motion Induced by Polarized Light. *Nat. Commun.* **2015**, *6*, No. 6594.
- (14) Rubio-Marcos, F.; Ochoa, D. A.; Del Campo, A.; Garcia, M. A.; Castro, G. R.; Fernandez, J. F.; Garcia, J. E. Reversible Optical Control of Macroscopic Polarization in Ferroelectrics. *Nat. Photonics* **2018**, *12*, 29–32.
- (15) Belianinov, A.; He, Q.; Dziaugys, A.; Maksymovych, P.; Eliseev, E.; Borisevich, A.; Morozovska, A.; Banys, J.; Vysochanskii, Y.; Kalinin, S. V. Cuinp2s6 Room Temperature Layered Ferroelectric. *Nano Lett.* **2015**, *15*, 3808–3814.
- (16) Liu, F.; You, L.; Seyler, K. L.; Li, X.; Yu, P.; Lin, J.; Wang, X.; Zhou, J.; Wang, H.; He, H.; et al. Room-Temperature Ferroelectricity in Cuinp2s6 Ultrathin Flakes. *Nat. Commun.* **2016**, *7*, No. 12357.
- (17) Yuan, S. G.; Luo, X.; Chan, H. L.; Xiao, C. C.; Dai, Y. W.; Xie, M. H.; Hao, J. H. Room-Temperature Ferroelectricity in Mote2 Down to the Atomic Monolayer Limit. *Nat. Commun.* **2019**, *10*, No. 1775.
- (18) Fei, Z. Y.; Zhao, W. J.; Palomaki, T. A.; Sun, B. S.; Miller, M. K.; Zhao, Z. Y.; Yan, J. Q.; Xu, X. D.; Cobden, D. H. Ferroelectric Switching of a Two-Dimensional Metal. *Nature* **2018**, *560*, 336–339. (19) Si, M.; Saha, A. K.; Gao, S.; Qiu, G.; Qin, J.; Duan, Y.; Jian, J.; Niu, C.; Wang, H.; Wu, W.; et al. A Ferroelectric Semiconductor Field-Effect Transistor. *Nat. Electron.* **2019**, *2*, 580–586.
- (20) Si, M.; Saha, A. K.; Liao, P.-Y.; Gao, S.; Neumayer, S. M.; Jian, J.; Qin, J.; Balke Wisinger, N.; Wang, H.; Maksymovych, P.; et al. Room-Temperature Electrocaloric Effect in Layered Ferroelectric Cuinp2s6 for Solid-State Refrigeration. *ACS Nano* **2019**, *13*, 8760–8765.
- (21) Wang, X.; Liu, C.; Chen, Y.; Wu, G.; Yan, X.; Huang, H.; Wang, P.; Tian, B.; Hong, Z.; Wang, Y.; et al. Ferroelectric Fet for

- Nonvolatile Memory Application with Two-Dimensional Mose2 Channels. 2D Mater. 2017, 4, No. 025036.
- (22) Gong, C.; Kim, E. M.; Wang, Y.; Lee, G.; Zhang, X. Multiferroicity in Atomic Van Der Waals Heterostructures. *Nat. Commun.* **2019**, *10*, No. 2657.
- (23) Lyu, F. J.; Sun, Y. W.; Yang, Q.; Tang, B.; Li, M. Q.; Li, Z. W.; Sun, M.; Gao, P.; Ye, L. H.; Chen, Q. Thickness-Dependent Band Gap of  $\alpha$ -In2Se3: From Electron Energy Loss Spectroscopy to Density Functional Theory Calculations. *Nanotechnology* **2020**, *31*, No. 315711.
- (24) Zhou, Y.; Wu, D.; Zhu, Y.; Cho, Y.; He, Q.; Yang, X.; Herrera, K.; Chu, Z.; Han, Y.; Downer, M. C.; et al. Out-of-Plane Piezoelectricity and Ferroelectricity in Layered Alpha-In2se3 Nano-flakes. *Nano Lett.* **2017**, *17*, 5508–5513.
- (25) Cui, C.; Hu, W.-J.; Yan, X.; Addiego, C.; Gao, W.; Wang, Y.; Wang, Z.; Li, L.; Cheng, Y.; Li, P.; et al. Intercorrelated in-Plane and out-of-Plane Ferroelectricity in Ultrathin Two-Dimensional Layered Semiconductor In2se3. *Nano Lett.* **2018**, *18*, 1253–1258.
- (26) Xiao, J.; Zhu, H.; Wang, Y.; Feng, W.; Hu, Y.; Dasgupta, A.; Han, Y.; Wang, Y.; Muller, D. A.; Martin, L. W.; et al. Intrinsic Two-Dimensional Ferroelectricity with Dipole Locking. *Phys. Rev. Lett.* **2018**, *120*, No. 227601.
- (27) Zheng, C.; Yu, L.; Zhu, L.; Collins, J. L.; Kim, D.; Lou, Y.; Xu, C.; Li, M.; Wei, Z.; Zhang, Y.; et al. Room Temperature in-Plane Ferroelectricity in Van Der Waals In2se3. *Sci. Adv.* **2018**, *4*, No. eaar7720.
- (28) Ding, W. J.; Zhu, J. B.; Wang, Z.; Gao, Y. F.; Xiao, D.; Gu, Y.; Zhang, Z. Y.; Zhu, W. G. Prediction of Intrinsic Two-Dimensional Ferroelectrics in In2se3 and Other Iii2-Vi3 Van Der Waals Materials. *Nat. Commun.* **2017**, *8*, No. 14956.
- (29) Xue, F.; Hu, W.; Lee, K.-C.; Lu, L.-S.; Zhang, J.; Tang, H.-L.; Han, A.; Hsu, W.-T.; Tu, S.; Chang, W.-H.; et al. Room-Temperature Ferroelectricity in Hexagonally Layered Alpha-In2se3 Nanoflakes Down to the Monolayer Limit. *Adv. Funct. Mater.* **2018**, 28, No. 1803738, DOI: 10.1002/adfm.201803738.
- (30) Poh, S. M.; Tan, S. J. R.; Wang, H.; Song, P.; Abidi, I. H.; Zhao, X.; Dan, J.; Chen, J.; Luo, Z.; Pennycook, S. J.; et al. Molecular-Beam Epitaxy of Two-Dimensional In2se3 and Its Giant Electroresistance Switching in Ferroresistive Memory Junction. *Nano Lett.* **2018**, *18*, 6340–6346.
- (31) Wan, S.; Li, Y.; Li, W.; Mao, X.; Wang, C.; Chen, C.; Dong, J.; Nie, A.; Xiang, J.; Liu, Z.; et al. Nonvolatile Ferroelectric Memory Effect in Ultrathin  $\alpha$ -In2se3. *Adv. Funct. Mater.* **2019**, 29, No. 1808606, DOI: 10.1002/adfm.201808606.
- (32) Xue, F.; He, X.; Retamal, J. R. D.; Han, A.; Zhang, J.; Liu, Z.; Huang, J.; Hu, W.; Tung, V.; He, J.; et al. Gate-Tunable and Multidirection-Switchable Memristive Phenomena in a Van Der Waals Ferroelectric. *Adv. Mater.* **2019**, *31*, No. 1901300.
- (33) Wang, L.; Wang, X. J.; Zhang, Y. S.; Li, R. L.; Ma, T.; Leng, K.; Chen, Z.; Abdelwahab, I.; Loh, K. P. Exploring Ferroelectric Switching in Alpha-in(2)Se(3)for Neuromorphic Computing. *Adv. Funct. Mater.* **2020**, 30, No. 2004609, DOI: 10.1002/adfm.202004609.
- (34) Parker, J.; Gu, Y. Highly Efficient Polarization-Controlled Electrical Conductance Modulation in a Van Der Waals Ferroelectric/Semiconductor Heterostructure. *Adv. Electron. Mater.* **2022**, 8, No. 2200413.
- (35) Xu, K.; Jiang, W.; Gao, X. S.; Zhao, Z. J.; Low, T.; Zhu, W. J. Optical Control of Ferroelectric Switching and Multifunctional Devices Based on Van Der Waals Ferroelectric Semiconductors. *Nanoscale* **2020**, *12*, 23488–23496.
- (36) Xue, F.; He, X.; Liu, W.; Periyanagounder, D.; Zhang, C.; Chen, M.; Lin, C.; Luo, L.; Yengel, E.; Tung, V.; et al. Optoelectronic Ferroelectric Domain-Wall Memories Made from a Single Van Der Waals Ferroelectric. *Adv. Funct. Mater.* **2020**, *30*, No. 2004206.
- (37) Gabel, M.; Gu, Y. Understanding Microscopic Operating Mechanisms of a Van Der Waals Planar Ferroelectric Memristor. *Adv. Funct. Mater.* **2021**, *31*, No. 2009999.

- (38) Igo, J.; Gabel, M.; Yu, Z. G.; Yang, L. L.; Guo, Y. Photodefined in-Plane Heterostructures in Two-Dimensional In2se3 Nanolayers for Ultrathin Photodiodes. ACS Appl. Nano Mater. 2019, 2, 6774–6782.
- (39) Sidorkin, A. S. Domain Structure in Ferroelectrics and Related Materials; Cambridge International Science Publishing, 2006.
- (40) Schoenherr, P.; Shapovaloy, K.; Schaab, J.; Yan, Z.; Bourret, E. D.; Hentschel, M.; Stengel, M.; Fiebig, M.; Cano, A.; Meier, D. Observation of Uncompensated Bound Charges at Improper Ferroelectric Domain Walls. *Nano Lett.* **2019**, *19*, 1659–1664.
- (41) Tang, W.; Zhang, X.; Yu, H.; Gao, L.; Zhang, Q.; Wei, X.; Hong, M.; Gu, L.; Liao, Q.; Kang, Z.; et al. A Van Der Waals Ferroelectric Tunnel Junction for Ultrahigh-Temperature Operation Memory. *Small Methods* **2022**, *6*, No. 2101583.
- (42) Zhai, Y. B.; Xie, P.; Hu, J. H.; Chen, X.; Feng, Z. H.; Lv, Z. Y.; Ding, G. L.; Zhou, K.; Zhou, Y.; Han, S. T. Reconfigurable 2d-Ferroelectric Platform for Neuromorphic Computing. *Appl. Phys. Rev.* **2023**, *10*, No. 011408.